Prospects for Applied Mathematics and Data Analysis

♦ **ISSN:** 2836-4449 **Vol:** 06, No. 01, 2026 ♦ PP. 01–06

♦ **Article DOI:** https://doi.org/10.54216/PAMDA.060101

FULL LENGTH ARTICLE

Spectrally Matched Fractional Sobolev Tikhonov Regularization for Periodic Deconvolution

Takaaki Fujita[1,*] **Ajoy Kanti Das**[2]

[1] Independent Researcher, Tokyo, Japan

[2] Associate Professor, Department of Mathematics, Tripura University, Agartala-799022, Tripura, India

Emails: Takaaki.fujita060@gmail.com; ajoykantidas@gmail.com

Received: September 14, 2025 Revised: November 20, 2025 Accepted: January 09, 2026 ⋆ Corresponding author

ABSTRACT

Let $\mathbb{T}=\mathbb{R}/\mathbb{Z}$ and $A_\beta=(I-\Delta)^{-\beta/2}$ with $\beta>0$. From data

$$g^\delta=A_\beta f^\dagger+\eta, \qquad \|\eta\|_2\le\delta,$$

consider the fractional Sobolev Tikhonov family

$$f^\delta_{\lambda,s}=\arg\min_{f\in H^s(\mathbb{T})}\left\{\left\|A_\beta f-g^\delta\right\|_2^2+\lambda\,\|f\|_{H^s}^2\right\},\qquad s\ge 0.$$

Writing $\mu_k=(1+4\pi^2k^2)^{1/2}$ and $\rho=s+\beta$, the estimator is diagonal in the Fourier basis,

$$\widehat{f^\delta_{\lambda,s}}(k)=\frac{\mu_k^\beta}{1+\lambda\mu_k^{2\rho}}\,\widehat{g^\delta}(k).$$

If $f^\dagger\in H^r(\mathbb{T})$ and $0<r\le 2\rho$, then

$$\left\|f^\delta_{\lambda,s}-f^\dagger\right\|_2\le C_a\delta\lambda^{-a}+C_bM_r\lambda^b,$$
$$a=\frac{\beta}{2\rho},\qquad b=\frac{r}{2\rho},\qquad M_r=\left\|f^\dagger\right\|_{H^r}.$$

where $C_q=q^q(1-q)^{1-q}$ for $0<q<1$ and $C_1=1$. Direct minimization gives $\lambda_*\asymp\delta^{2\rho/(r+\beta)}$ and

$$\left\|f^\delta_{\lambda_*,s}-f^\dagger\right\|_2=O\left(\delta^{r/(r+\beta)}\right).$$

Thus the pre-saturation exponent is independent of the penalty order s. When $r>2\rho$, the bias saturates and the rate becomes $O(\delta^{2\rho/(2\rho+\beta)})$; hence the least order avoiding saturation is $s_{\min}=\max\{0,r/2-\beta\}$. The balanced half-power frequency satisfies $\mu_c\asymp\delta^{-1/(r+\beta)}$, whereas its logarithmic roll-off is $-\rho/2$. The same exponents persist for spectrally equivalent convolution operators $c_-\mu_k^{-\beta}\le a_k\le c_+\mu_k^{-\beta}$. Fourier experiments on $N=2048$ modes, using three source regularities, four penalty orders, five noise levels, and 30 perturbations per configuration, reproduce the predicted saturation ordering and transition boundary. For the H^6 benchmark at $\delta=10^{-3}$, the mean L^2 error decreases from 1.4013×10^{-2} for $s=0$ to 1.2710×10^{-3} for $s=2$; the latter is the first tested order in the non-saturated regime.

Keywords: Inverse problems ▪ Spectral regularization ▪ Fractional Sobolev spaces ▪ Tikhonov regularization ▪ Deconvolution ▪ Hilbert scales ▪ Convergence rates ▪ Saturation

1. PROBLEM FORMULATION AND SPECTRAL SETTING

For a smoothing inverse problem, the regularization error is controlled by three spectral laws: decay of the forward singular values, growth of the penalty weights, and decay of the coefficients of the unknown. If these laws are represented by powers $\mu^{-\beta}$, μ^{2s}, and μ^{-r}, respectively, then the combined exponent

$$\rho = s+\beta$$

sets both stability loss and regularizer qualification. Hilbert- and Banach-scale analyses, oversmoothing theory, statistical inverse learning, ensemble inversion, and variational regularization treat these mechanisms under broader assumptions [1, 2, 3, 4, 5, 6, 7, 8]. Matrix-function, optimal-transport, hybrid-projection, and learned regularization methods provide complementary computational constructions [9, 10, 11, 12, 13, 14, 15]. Here the common spectral structure is made explicit for a fractional Sobolev penalty, allowing the roles of s, β, and r to be separated algebraically.

Let $\mathbb{T} = \mathbb{R}/\mathbb{Z}$ and $e_k(x) = e^{2\pi ikx}$. Set

$$\mu_k = (1+4\pi^2k^2)^{1/2}, \qquad \|f\|^2_{H^q} = \sum_{k\in\mathbb{Z}} \mu_k^{2q}|\widehat{f}(k)|^2.$$

The forward family is diagonal,

$$A_\beta e_k = \mu_k^{-\beta} e_k, \qquad \beta > 0, \tag{1}$$

so that A_β loses β derivatives. Noisy data obey

$$g^\delta = A_\beta f^\dagger + \eta, \qquad \|\eta\|_2 \le \delta. \tag{2}$$

Such power-decaying singular systems are a standard laboratory for spectral regularization, statistical inverse problems, and fractional inverse diffusion [16, 17].

For $s \ge 0$ consider

$$\mathscr{J}_{\lambda,s}(f) = \left\|A_\beta f - g^\delta\right\|_2^2 + \lambda\,\|f\|^2_{H^s}, \qquad \lambda > 0. \tag{3}$$

The analysis below gives the rational reconstruction filter and, for $0 < r \le 2(s+\beta)$, the two order-invariant scalings

$$\left\|f^\delta_{\lambda_*,s} - f^\dagger\right\|_2 = O\left(\delta^{r/(r+\beta)}\right), \qquad \mu_c \asymp \delta^{-1/(r+\beta)}.$$

The penalty order acts through qualification and filter geometry: it moves the saturation threshold from 2β to $2(s+\beta)$ and changes the logarithmic slope at the half-power frequency to $-(s+\beta)/2$. These identities yield the matching rule

$$s_{\min}(r,\beta) = \max\left\{0, \frac{r}{2} - \beta\right\}, \tag{4}$$

which is the smallest Sobolev order that prevents regularity loss through saturation.

All estimates are derived from the exact periodic multipliers rather than asymptotic singular-value replacements. This isolates, in closed form, the saturation mechanism studied in more general Hilbert- and Banach-scale settings [18, 5, 8]. Manufactured states with prescribed Fourier decay are then used to measure the predicted exponents against known ground truth.

2. SPECTRAL REPRESENTATION AND ERROR BOUNDS

2.1 Exact minimizer

The diagonal structure makes the minimization in (3) separable. This is useful because all stability constants can be obtained from one-dimensional scalar extrema rather than unspecified operator constants.

Theorem 1 (Exact reconstruction multiplier)**.** *For $s \ge 0$ and $\lambda > 0$, (3) has a unique minimizer in $H^s(\mathbb{T})$. Its Fourier coefficients are*

$$\widehat{f}^\delta_{\lambda,s}(k) = R_{\lambda,s}(\mu_k)\widehat{g}^\delta(k), \qquad R_{\lambda,s}(\mu) = \frac{\mu^\beta}{1+\lambda\mu^{2\rho}}, \tag{5}$$

where $\rho = s+\beta$. With exact data, the corresponding truth filter is

$$F_{\lambda,s}(\mu) = \frac{1}{1+\lambda\mu^{2\rho}}. \tag{6}$$

Proof. Parseval's identity gives

$$\mathscr{J}_{\lambda,s}(f) = \sum_k \left(|\mu_k^{-\beta}\widehat{f}(k) - \widehat{g}^\delta(k)|^2 + \lambda\mu_k^{2s}|\widehat{f}(k)|^2\right).$$

Each summand is strictly convex. Setting its complex derivative to zero yields $(\mu_k^{-2\beta} + \lambda\mu_k^{2s})\widehat{f}(k) = \mu_k^{-\beta}\widehat{g}^\delta(k)$, which reduces to (5). Substituting $\widehat{g}(k) = \mu_k^{-\beta}\widehat{f}^\dagger(k)$ gives (6). Strict positivity of $\mu_k^{-2\beta} + \lambda\mu_k^{2s}$ proves uniqueness. □

Equation (5) separates two different responses. The inverse factor μ^β restores attenuated modes, while $(1+\lambda\mu^{2\rho})^{-1}$ suppresses the modes at which this restoration becomes unstable. Increasing s raises ρ; it therefore changes the shape of the suppressing factor even when the forward operator is unchanged.

2.2 The two error mechanisms

Write $R_{\lambda,s}g^\delta = f^\delta_{\lambda,s}$. From (2),

$$f^\delta_{\lambda,s} - f^\dagger = R_{\lambda,s}\eta - (I - F_{\lambda,s})f^\dagger. \tag{7}$$

The first term is noise amplification; the second is deterministic bias.

Lemma 1 (Noise amplification)**.** *Let $a = \beta/(2\rho) \in (0,1/2]$. Then*

$$\|R_{\lambda,s}\|_{L^2\to L^2} \le C_a\lambda^{-a}, \qquad C_a = a^a(1-a)^{1-a}. \tag{8}$$

Proof. For $z = \lambda\mu^{2\rho}$,

$$R_{\lambda,s}(\mu) = \lambda^{-a}\frac{z^a}{1+z}.$$

The continuous supremum of $z^a/(1+z)$ over $z > 0$ occurs at $z = a/(1-a)$ and equals $a^a(1-a)^{1-a}$. Taking the supremum over the discrete set $\{\mu_k\}$ cannot increase it. □

Lemma 2 (Bias before saturation)**.** *Assume $f^\dagger \in H^r(\mathbb{T})$ and $0 < r \le 2\rho$. With $b = r/(2\rho) \in (0,1]$,*

$$\left\|(I - F_{\lambda,s})f^\dagger\right\|_2 \le C_b \lambda^b \left\|f^\dagger\right\|_{H^r}, \qquad C_b = b^b(1-b)^{1-b}, \tag{9}$$

where $C_1 = 1$.

Proof. By Parseval,

$$\left\|(I - F)f^\dagger\right\|_2 \le \sup_{\mu \ge 1} \frac{\lambda \mu^{2\rho - r}}{1 + \lambda \mu^{2\rho}} \left\|f^\dagger\right\|_{H^r}.$$

Setting $z = \lambda \mu^{2\rho}$ transforms the scalar factor into $\lambda^b z^{1-b}/(1+z)$. Its maximum is $C_b \lambda^b$; the endpoint $b = 1$ follows by monotonicity. □

Lemmas 1 and 2 determine the complete bias–stability trade-off.

3. RATE INVARIANCE AND SATURATION

Theorem 2 (Balanced error law)**.** *Let $f^\dagger \in H^r(\mathbb{T})$ with $0 < r \le 2(s+\beta)$ and set $M_r = \left\|f^\dagger\right\|_{H^r}$. Then*

$$\left\|f^\delta_{\lambda,s} - f^\dagger\right\|_2 \le C_a \delta \lambda^{-a} + C_b M_r \lambda^b, \tag{10}$$

where $a = \beta/(2\rho)$ and $b = r/(2\rho)$. The minimizer of the right-hand side is

$$\lambda_* = \left(\frac{a C_a \delta}{b C_b M_r}\right)^{1/(a+b)}, \tag{11}$$

and, with

$$\kappa_{a,b} = \left(\frac{b}{a}\right)^{a/(a+b)} + \left(\frac{a}{b}\right)^{b/(a+b)},$$

$$\begin{aligned}\left\|f^\delta_{\lambda_*,s} - f^\dagger\right\|_2 &\le \kappa_{a,b}(C_a\delta)^{b/(a+b)}(C_b M_r)^{a/(a+b)} \\ &= O\left(\delta^{\frac{r}{r+\beta}}\right).\end{aligned} \tag{12}$$

In particular, the exponent of δ in (12) does not depend on s.

Proof. Equation (10) is (7) combined with Lemmas 1–2. Differentiating its right-hand side gives $b C_b M_r \lambda^{b-1} = a C_a \delta \lambda^{-a-1}$ and hence (11). Since $b/(a+b) = r/(r+\beta)$, substitution yields (12). □

The cancellation of $\rho = s + \beta$ in $b/(a+b)$ is the first structural invariance. It says that increasing s cannot improve the asymptotic exponent when the truth is already inside the non-saturated range. This does not mean that s is irrelevant: the constants, the balanced value of λ, and the filter geometry all change.

Proposition 1 (Saturation boundary)**.** *If $r > 2\rho$ and $f^\dagger \in H^r(\mathbb{T})$, then the bias admits the saturated estimate*

$$\left\|(I - F_{\lambda,s})f^\dagger\right\|_2 \le \lambda \left\|f^\dagger\right\|_{H^{2\rho}}. \tag{13}$$

Let $M_{2\rho} = \left\|f^\dagger\right\|_{H^{2\rho}}$. Balancing (13) with (8) gives

$$\lambda_{\text{sat}} = \left(\frac{a C_a \delta}{M_{2\rho}}\right)^{1/(a+1)},$$

and therefore

$$\left\|f^\delta_{\lambda_{\text{sat}},s} - f^\dagger\right\|_2 \le \kappa_{a,1}(C_a\delta)^{1/(a+1)} M_{2\rho}^{a/(a+1)} = O\left(\delta^{\frac{2\rho}{2\rho+\beta}}\right). \tag{14}$$

Thus the source regularity r enters the exponent only until $r = 2(s+\beta)$.

Proof. Since $z/(1+z) \le z$, the exact-data bias multiplier satisfies $1 - F_{\lambda,s}(\mu) \le \lambda \mu^{2\rho}$, proving (13). The balance has exponents $a = \beta/(2\rho)$ and $b = 1$, so $b/(a+b) = 2\rho/(2\rho+\beta)$. □

Corollary 1 (Regularity-matched order)**.** *To avoid saturation for a source class H^r, it is sufficient and, within the present family, minimal to choose*

$$s \ge s_{\min}(r,\beta) = \max\{0, r/2 - \beta\}.$$

Corollary 1 identifies the asymptotic role of the fractional order: it matches regularizer qualification to source smoothness rather than merely increasing smoothing. Related saturation and oversmoothing questions are central in modern Tikhonov theory [1, 3, 4, 5]; here the periodic multiplier makes the threshold explicit.

4. SPECTRAL CUTOFF AND PENALTY-ORDER EFFECTS

Define the half-power transition frequency by

$$\lambda \mu_c^{2\rho} = 1, \qquad \mu_c = \lambda^{-1/(2\rho)}. \tag{15}$$

This quantity is not an imposed truncation. It is the intrinsic frequency at which $F_{\lambda,s} = 1/2$.

Proposition 2 (Cutoff invariance and transition slope)**.** *Under the non-saturated balance (11),*

$$\mu_c \asymp \delta^{-1/(r+\beta)}, \tag{16}$$

which is independent of s. Moreover,

$$\left.\frac{dF_{\lambda,s}}{d\log\mu}\right|_{\mu=\mu_c} = -\frac{\rho}{2} = -\frac{s+\beta}{2}. \tag{17}$$

Proof. Equation (11) has $\lambda_* \asymp \delta^{1/(a+b)} = \delta^{2\rho/(r+\beta)}$; insertion in (15) gives (16). For $z = \lambda\mu^{2\rho}$, $dF/d\log\mu = -2\rho z/(1+z)^2$. At the cutoff $z = 1$, giving (17). □

Before saturation, changing s leaves the asymptotic location of the resolved bandwidth unchanged after balancing, but changes the sharpness of the transition from resolved to suppressed modes. Figure 1 visualizes this distinction for the parameters used in the numerical experiment.

A related spectral requirement appears in plug-and-play regularization, where denoising operators are constrained to retain convergence and stability properties [14]. Here the filter acts

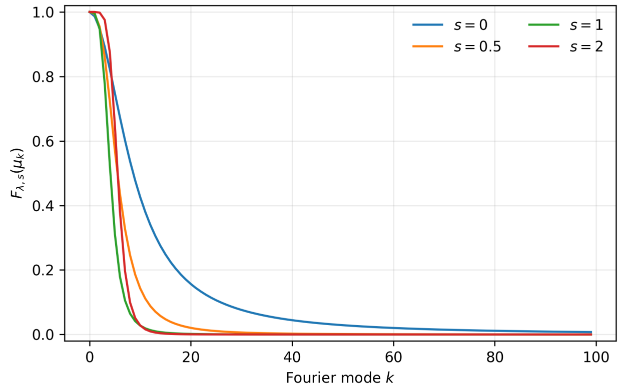

Figure 1. Exact-data filters $F_{\lambda,s}$ for the high-regularity benchmark at $\delta = 10^{-3}$ using the theoretical balanced parameter. Larger s changes the transition geometry and, for this source, eventually removes saturation.

directly on the inverse multiplier, and stability is likewise determined by spectral growth.

4.1 Robustness under spectral equivalence

The exact Bessel-potential symbol in (1) is not essential for the rate exponents. Suppose instead that a self-adjoint positive convolution operator A satisfies

$$c_-\mu_k^{-\beta} \le a_k \le c_+\mu_k^{-\beta}, \qquad Ae_k = a_k e_k, \tag{18}$$

for constants $0 < c_- \le c_+ < \infty$. The regularized coefficient becomes

$$\widehat{f}^{\delta}_{\lambda,s}(k) = \frac{a_k}{a_k^2 + \lambda\mu_k^{2s}}\widehat{g}^{\delta}(k).$$

Thus the preceding calculus survives without requiring an exact power law.

Proposition 3 (Exponent stability under equivalent spectra)**.** *Assume (18), $f^\dagger \in H^r$, and $0 < r \le 2(s+\beta)$. With $a = \beta/(2\rho)$ and $b = r/(2\rho)$,*

$$\|R_{\lambda,s}\|_{2\to 2} \le c_+ c_-^{2a-2} C_a \lambda^{-a}, \tag{19}$$

$$\|(I - F_{\lambda,s})f^\dagger\|_2 \le c_-^{-2b} C_b \lambda^b \|f^\dagger\|_{H^r}. \tag{20}$$

Consequently, balancing the two terms again gives the exponent $r/(r+\beta)$ and the cutoff scaling $\delta^{-1/(r+\beta)}$ up to constants.

Proof. For the noise multiplier,

$$\frac{a_k}{a_k^2 + \lambda\mu_k^{2s}} \le \frac{c_+\mu_k^{\beta}}{c_-^2 + \lambda\mu_k^{2\rho}}.$$

With $z = (\lambda/c_-^2)\mu_k^{2\rho}$, Lemma 1 gives (19). Similarly,

$$1 - F_{\lambda,s}(\mu_k) = \frac{\lambda\mu_k^{2s}}{a_k^2 + \lambda\mu_k^{2s}} \le \frac{(\lambda/c_-^2)\mu_k^{2\rho}}{1 + (\lambda/c_-^2)\mu_k^{2\rho}},$$

and the scalar maximization in Lemma 2 yields (20). Only multiplicative constants have changed, so the balance exponents are unchanged. □

Proposition 3 extends the rate law to polynomially smoothing convolution operators with two-sided spectral equivalence. It also gives a sufficient mechanism by which matrix or projection approximations retain the same rate exponents when their spectral distortion is uniformly bounded [9, 12].

5. NUMERICAL VERIFICATION OF THE RATE LAW

5.1 Construction

Numerical verification is carried out on a periodic grid with $N = 2048$ equispaced points and $\beta = 1$. Manufactured states are used so that $f^\dagger$, the exact error, and source regularity are known. Three deterministic real-valued states are generated by conjugate-symmetric Fourier coefficients

$$|\widehat{f}_r(k)| \propto k^{-(r+0.70)}, \qquad r \in \{0.75, 3, 6\}, \quad k \neq 0, \tag{21}$$

with fixed nontrivial phases and a nonzero mean, followed by L^2 normalization. This decay guarantees $f_r \in H^r$ while retaining a long spectral tail.

For each state, exact observations are generated by (1). Gaussian perturbation vectors are independently sampled and rescaled so that their discrete L^2 norm equals

$$\delta \in \{10^{-2}, 3\times 10^{-3}, 10^{-3}, 3\times 10^{-4}, 10^{-4}\}.$$

For every (r, δ, s) with $s \in \{0, 0.5, 1, 2\}$, 30 perturbations are reconstructed. The parameter λ is computed from (11): H^r is used in the non-saturated regime and $H^{2\rho}$ in the saturated regime. Reconstruction error is not used to tune λ. The random generator seed is 20260115; a separate oracle grid is retained only for diagnostic comparison.

The forward operator, truth, noise norm, and parameter rule are fully specified, as in contemporary computational regularization studies [12, 15]. The supplementary package contains the code, generated samples, replicate-level errors, parameter values, and plotted data.

5.2 Saturation diagram

Table 1 compares empirical log–log slopes of mean error against the theoretical exponent. For $r = 6$, the sequence of predicted exponents increases from $2/3$ to $3/4$ to $4/5$ while $s = 0, 0.5, 1$ remain saturated; at $s = 2$, $2(s+\beta) = 6$ reaches the source regularity and the non-saturated prediction becomes $6/7$. The empirical slopes reproduce the ordering and the transition boundary. The $r = 6$, $s = 2$ case remains visibly pre-asymptotic: its observed slope is 0.775 rather than the limiting value $6/7 \approx 0.857$. Here the balanced λ is very small, so the finite grid leaves a broad passband at the tested noise levels.

For the low-regularity state, all four penalty orders are non-saturated and the theorem predicts the same exponent $0.75/(1.75) = 0.4286$. The measured slopes 0.472–0.503 differ in finite range but do not exhibit the systematic order-dependent increase seen for the smooth source. This behavior is consistent with the order-invariant exponent in Theorem 2.

5.3 Error levels for a smooth source

Table 2 gives the mean L^2 error for $r = 6$. The effect of order matching is already substantial over the tested noise range: at $\delta = 10^{-3}$ the $s = 2$ error is roughly one eleventh of the $s = 0$ error. The difference should not be interpreted

Table 1. Empirical and theoretical convergence exponents.

r	s	Regime	Empirical	Theory
0.75	0.0	non-sat.	0.472	0.429
0.75	0.5	non-sat.	0.493	0.429
0.75	1.0	non-sat.	0.499	0.429
0.75	2.0	non-sat.	0.503	0.429
3.00	0.0	saturated	0.633	0.667
3.00	0.5	non-sat.	0.697	0.750
3.00	1.0	non-sat.	0.769	0.750
3.00	2.0	non-sat.	0.763	0.750
6.00	0.0	saturated	0.638	0.667
6.00	0.5	saturated	0.736	0.750
6.00	1.0	saturated	0.789	0.800
6.00	2.0	non-sat.	0.775	0.857

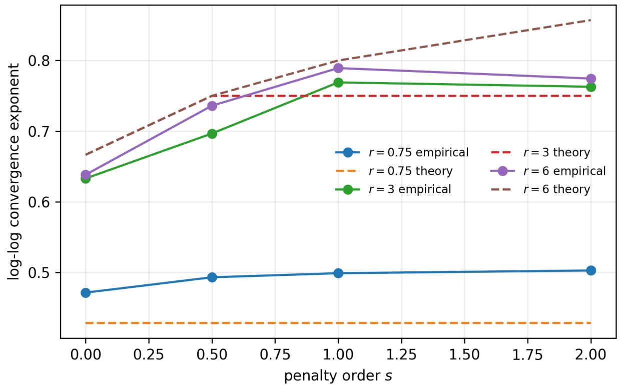

Figure 2. Measured log–log exponents and the theoretical saturation diagram. The rough source has one common pre-saturation rate; the smooth source gains rate as the penalty qualification increases.

as a contradiction of rate invariance, because $s = 0, 0.5, 1$ are precisely the saturated cases for $r = 6$.

A representative reconstruction at $\delta = 10^{-3}$ is shown in Figure 4. The data themselves are blurred, not merely noisy; hence direct comparison between g^δ and $f^\dagger$ also displays the smoothing action of A_β. The $s = 2$ reconstruction retains the resolved oscillatory content while suppressing the high-frequency inverse amplification.

6. SCOPE OF THE SPECTRAL RESULT

The periodic operator separates the three relevant scales exactly: smoothing order, penalty order, and source smoothness. Proposition 3 shows that the resulting exponents do not depend on the exact multiplier $\mu^{-\beta}$, provided a two-sided polynomial spectral bound is retained. General Hilbert-scale, statistical, and variational theories obtain related order-optimality statements under substantially broader assumptions [2, 8, 17]; Banach-space results show that oversmoothing can likewise be treated without requiring the exact solution to lie in the penalty domain [4, 5]. Within this spectral model, the penalty order cancels from the pre-saturation error exponent and the balanced cutoff exponent, while remaining explicitly in the qualification threshold and transition slope.

A higher-order penalty is therefore not uniformly preferable. If r is low, raising s cannot improve $r/(r+\beta)$ and may alter constants unfavorably. If r exceeds $2(s+\beta)$, however, a low-order penalty has insufficient qualification and its rate is capped by (14). In that case (4) raises the qualification just enough to recover the source-limited rate. The numerical results mirror this division.

Table 2. Mean L^2 reconstruction error for $r = 6$ (30 perturbations).

δ	$s=0$	$s=.5$	$s=1$	$s=2$
10^{-2}	0.060354	0.033463	0.022714	0.007102
3×10^{-3}	0.028502	0.014116	0.009036	0.003050
10^{-3}	0.014013	0.006210	0.003729	0.001271
3×10^{-4}	0.006487	0.002568	0.001454	0.000471
10^{-4}	0.003206	0.001133	0.000602	0.000209

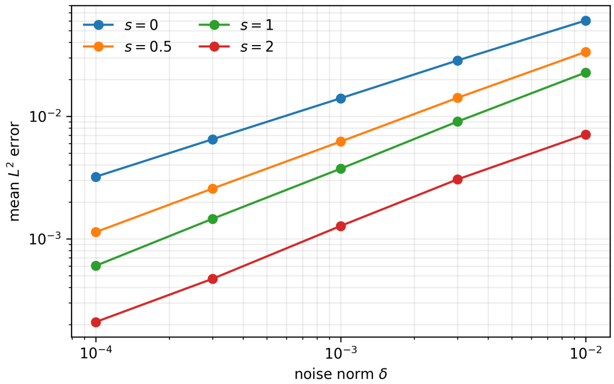

Figure 3. Mean reconstruction error versus noise norm for the H^6 benchmark. Increasing s moves the estimator through successive saturation thresholds.

Several extensions require additional machinery. Noncommuting penalties and forward operators destroy the scalar multiplier argument. Nonperiodic boundaries change the eigensystem and may couple discretization error to regularization error. Unknown source smoothness makes (11) unavailable directly and calls for discrepancy, balancing or adaptive rules, a question treated in broader deterministic and statistical frameworks [19, 7, 6, 20]. Nonquadratic regularizers introduce geometry not visible in the present Hilbert model; contemporary examples include optimal-transport and nonsmooth convex penalties [11, 21]. Finally, learned priors can improve empirical reconstructions but require a separate argument to retain the regularization property [13, 14].

The advantage of the present model is that every exponent in the bias–noise tradeoff is explicit and every numerical quantity is reproducible from known ground truth.

7. CONCLUSION

For $A_\beta = (I-\Delta)^{-\beta/2}$, the fractional Sobolev Tikhonov estimator is governed by

$$R_{\lambda,s}(\mu) = \frac{\mu^\beta}{1+\lambda\mu^{2(s+\beta)}}.$$

Its noise amplification is $O(\lambda^{-\beta/[2(s+\beta)]})$ and, for $0 < r \le 2(s+\beta)$, its H^r bias is $O(\lambda^{r/[2(s+\beta)]})$. Their balance gives

$$\lambda_* \asymp \delta^{2(s+\beta)/(r+\beta)}, \qquad \left\| f^\delta_{\lambda_*,s} - f^\dagger \right\|_2 = O\left(\delta^{r/(r+\beta)}\right),$$

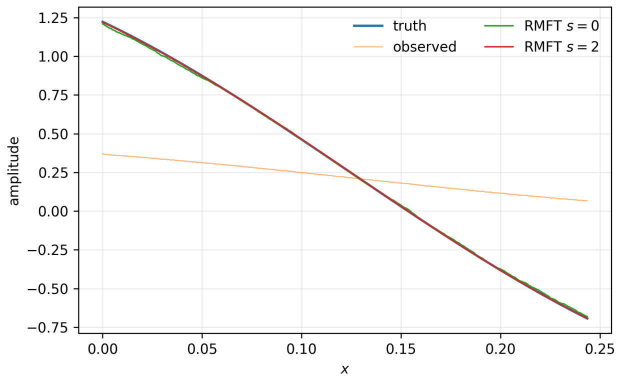

Figure 4. Representative portion of the $r = 6$ reconstruction for $\delta = 10^{-3}$. The observation is the smoothed noisy datum; the two curves use the theoretical parameter rule.

with balanced cutoff $\mu_c \asymp \delta^{-1/(r+\beta)}$. The penalty order does not enter these two pre-saturation exponents. It enters through qualification: the boundary is $r = 2(s+\beta)$, the cutoff slope is $-(s+\beta)/2$, and the least order avoiding saturation is $\max\{0, r/2 - \beta\}$. The numerical results reproduce this transition and quantify the finite-grid deviation from the asymptotic slope in the highest-order case.

REFERENCES

[1] A. Rastogi, "Tikhonov regularization with oversmoothing penalty for nonlinear statistical inverse problems," *Communications on Pure and Applied Analysis*, vol. 19, no. 8, pp. 4111–4126, 2020.

[2] A. Rastogi, G. Blanchard, and P. Mathé, "Convergence analysis of tikhonov regularization for non-linear statistical inverse problems," *Electronic Journal of Statistics*, vol. 14, no. 2, pp. 2798–2841, 2020.

[3] B. Hofmann and R. Plato, "Convergence results and low-order rates for nonlinear tikhonov regularization with oversmoothing penalty term," *Electronic Transactions on Numerical Analysis*, vol. 53, pp. 313–328, 2020.

[4] D.-H. Chen, B. Hofmann, and I. Yousept, "Oversmoothing tikhonov regularization in banach spaces," *Inverse Problems*, vol. 37, no. 8, p. 085007, 2021.

[5] P. Miller and T. Hohage, "Convergence rates for oversmoothing banach space regularization," *Electronic Transactions on Numerical Analysis*, vol. 57, pp. 101–126, 2022.

[6] T. Hohage and F. Werner, "Error estimates for variational regularization of inverse problems with general noise models for data and operator," *Electronic Transactions on Numerical Analysis*, vol. 57, pp. 127–152, 2022.

[7] F. Parzer and O. Scherzer, "On convergence rates of adaptive ensemble kalman inversion for linear ill-posed problems," *Numerische Mathematik*, vol. 152, pp. 371–409, 2022.

[8] A. Rastogi and P. Mathé, "Inverse learning in hilbert scales," *Machine Learning*, vol. 112, pp. 2469–2499, 2023.

[9] S. Cipolla, M. Donatelli, and F. Durastante, "Regularization of inverse problems by an approximate matrix-function technique," *Numerical Algorithms*, vol. 88, no. 3, pp. 1275–1308, 2021.

[10] K. Bredies and S. Fanzon, "An optimal transport approach for solving dynamic inverse problems in spaces of measures," *ESAIM: Mathematical Modelling and Numerical Analysis*, vol. 54, no. 6, pp. 2351–2382, 2020.

[11] K. Bredies, M. Carioni, S. Fanzon, and F. Romero, "A generalized conditional gradient method for dynamic inverse problems with optimal transport regularization," *Foundations of Computational Mathematics*, vol. 23, no. 3, pp. 833–898, 2023.

[12] J. Jiang, J. Chung, and E. de Sturler, "Hybrid projection methods with recycling for inverse problems," *SIAM Journal on Scientific Computing*, vol. 43, no. 5, pp. S146–S172, 2021.

[13] A. Habring and M. Holler, "A generative variational model for inverse problems in imaging," *SIAM Journal on Mathematics of Data Science*, vol. 4, no. 1, pp. 306–335, 2022.

[14] R. Cohen, M. Elad, and P. Milanfar, "Regularization by denoising via fixed-point projection (RED-PRO)," *SIAM Journal on Imaging Sciences*, vol. 14, no. 3, pp. 1374–1406, 2021.

[15] S. Gazzola and M. Sabaté Landman, "Regularization by inexact krylov methods with applications to blind deblurring," *SIAM Journal on Matrix Analysis and Applications*, vol. 42, no. 4, pp. 1528–1552, 2021.

[16] N. M. Dien, D. N. D. Hai, T. Q. Viet, and D. D. Trong, "On tikhonov's method and optimal error bound for inverse source problem for a time-fractional diffusion equation," *Computers & Mathematics with Applications*, vol. 80, no. 1, pp. 61–81, 2020.

[17] S. Lu, P. Niu, and F. Werner, "On the asymptotical regularization for linear inverse problems in presence of white noise," *SIAM/ASA Journal on Uncertainty Quantification*, vol. 9, no. 1, pp. 1–28, 2021.

[18] P. Miller and T. Hohage, "Maximal spaces for approximation rates in ℓ^1-regularization," *Numerische Mathematik*, vol. 149, no. 2, pp. 341–374, 2021.

[19] N. K. Chada, A. M. Stuart, and X. T. Tong, "Tikhonov regularization within ensemble kalman inversion," *SIAM Journal on Numerical Analysis*, vol. 58, no. 2, pp. 1263–1294, 2020.

[20] N. K. Chada, M. A. Iglesias, S. Lu, and F. Werner, "On a dynamic variant of the iteratively regularized gauss–newton method with sequential data," *SIAM Journal on Scientific Computing*, vol. 45, no. 6, pp. A3020–A3046, 2023.

[21] Y. Xia, W. Wang, and B. Han, "A fast averaged kaczmarz iteration with convex penalty for inverse problems in hilbert spaces," *SIAM Journal on Imaging Sciences*, vol. 15, no. 3, pp. 1079–1103, 2022.